Image pre-processing & data post-processing software dedicated to flow measurements in an automotive intake manifold

Dimitri Bonnet[1], David Ramel[1], Magali Barthes[1], Laurent Girardot[1], Yannick Bailly[1], Jean Stefanini[2], Anita Grenier[3], David Guyon[3]

[1] FEMTO-ST Institute, ENERGIE Department, BELFORT, France. yannick.bailly@univ-fcomte.fr
[2] TSI France Inc., MARSEILLE, France
[3] SOGEFI Group, Air&Cooling Systems – Engine Systems Division, Systèmes Moteurs SAS, France

ABSTRACT

The SIMBA project had for objective to model the whole air loop of the automotive engine. In order to get boundary conditions for this model and verify it, PIV measurements were done. Simultaneously in the eight intake manifold's runners of a DV6 TED4 PSA engine, acquisitions were obtained for each of the 720 crank angle degrees. Specific software (named PYV) was developed to pre-process images to deal with constraints inherent to running engine environment, and also to enable automate PIV processing.

1. INTRODUCTION

In the field of pollutant emissions (such as NOx and CO) related to terrestrial vehicles, standards are in constant evolution. The SIMBA project had for objective to model the whole air loop of the automotive engine. Boundary conditions of such a model required to be able to measure several fluidic parameters along the air loop. Our tasks were to achieve PIV measurements in the intake manifold's runners of a DV6 TED4 engine manufactured by PSA.
Optical measurements on a real running engine, in an industrial surrounding, are challenging. Most of optical velocity measurements were done over generic engines (mono-cylinder, or without firing...) [1, 2, 3, 4, 5]. Moreover, most of these measurements were performed in cylinders, and are still quite rare in the air loop [6, 7, 8].
We designed an optical system composed of a double cavity Nd:Yag laser, two cameras and 53 optical components to enable PIV measurements simultaneously in the eight intake manifold's runners of a diesel engine. This experimental setup is briefly presented in the next section.
When the engine was running, there were vibrations that induced spatial shifts between pairs of images acquired successively. Thus the spatial origin of each pair of images was not known precisely. As a consequence, the automation of PIV processing was not possible since the regions of interest could not have been precisely located. In order to automate PIV processing, it was necessary to develop software able to apply an offset to images (to obtain the same spatial reference on the images) and to correct their orientations. This pre-processing is detailed in the section 3.
Software was coded to enable different processings for multiple regions of interest in order to save time. Moreover, we coded a synthetic image generation program to validate our software. This is developed in section 4.
The fifth section presents some examples of experimental results for engine running at 2000 revolutions per minutes with a load of 70 N.m.

2. EXPERIMENTAL SETUP

To achieve optical measurements on a real running engine induced several constraints that had to be handled. These constraints mostly consisted in vibrations (that misalign optical devices), laser reflections in ducts (that deteriorate image quality) and engine bulk (that limit optical access). The strategy was to design an experimental setup to deal with most of the constraints, and then to solve residual issues with computing processings.

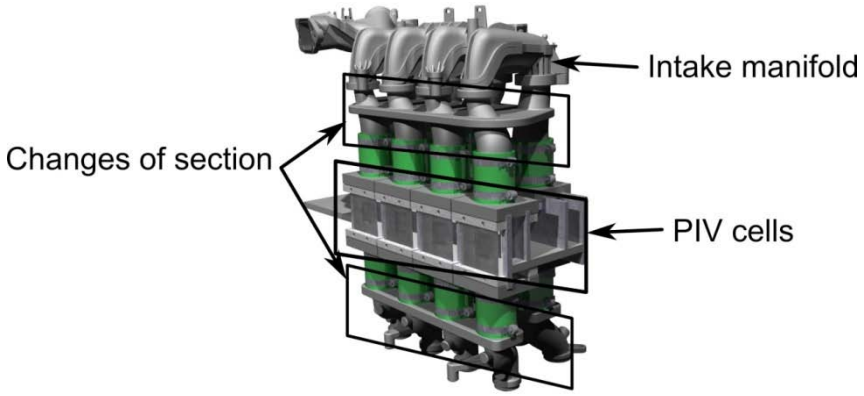

Figure 1 Modified intake manifold with optical access adaptations.

In order to obtain 8 velocity fields corresponding to 8 runners, 8 optical cells (shown on Figure 1) were inserted downstream the intake manifold. These cells were designed to gently change circular sections of the intake manifold into square ones, so that they enabled optical access while avoiding optical distortions. This was done using selective laser sintering technique. We used a single Quantel Evergreen double cavity Nd:Yag laser (532 nm wavelength) to create a laser sheet that was split into 8 identical laser sheets by means of various optical components (lenses, reflectors and beam splitters). This 8 laser sheets reached the 8 runners with the same optical path length. Pictures of the 8 fields were recorded by 2 TSI PIVCAM 13:8 cameras. Each camera visualized 4 fields corresponding to 4 runners of one side of the intake manifold. This was made possible by using 2 optical benches (composed with reflectors) and localized outside the engine. Each optical bench brings 4 images of 4 runners on a camera, with a same optical path length. All of these compounds (laser, cameras, optical benches and PIV cells) were interdependent with the engine to reduce vibrations influence. Principle of the optical installation is shown on Figure 2. Laser and cameras were triggered by a synchronizer so the 8 flows in the 8 runners were measured simultaneously.

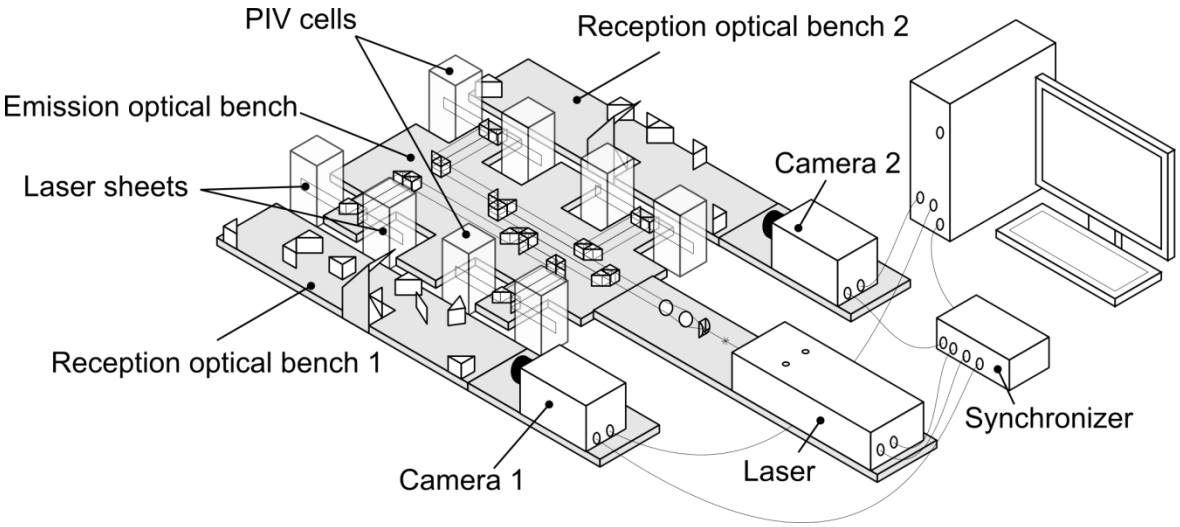

Figure 2 Principle of the optical installation.

With this setup, there was no optical distortion since visualization windows were plans. Moreover, laser reflections were limited as well as vibrations influence. Nevertheless, vibrations still induced a relative displacement between consecutive pairs of images as shown on Figure 3.

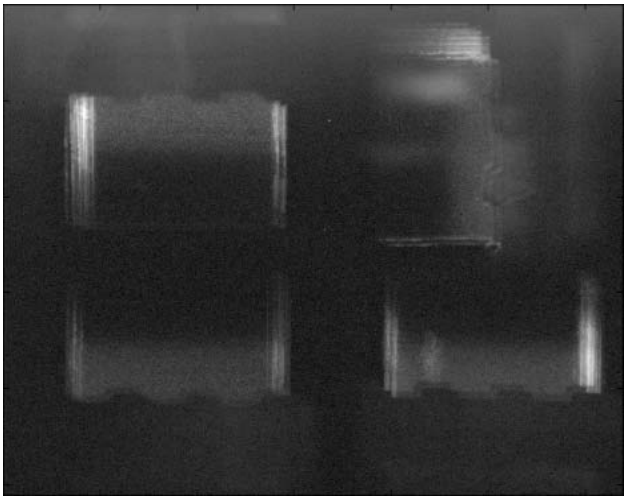

Figure 3 Consecutive pairs of images.

On this figure, two images, from a consecutive pair are superposed. One can observe the blur aspect due to a non identical spatial origin on both images. Furthermore, there still remained some reflections on the edges of the images. To deal with remaining issues, we decided to implement a pre-processing tool. This pre-processing, as well as the global image processing we applied, are presented in the next section.

3. PYV software

Software was Python coded and was designed with numerous features. PYV software was first developed to take into account the huge quantity of data that were obtained during experiments on the engine test bench. With 4 runners to be visualized on each camera, there were, on each image, different areas of interest. Thus software was developed in order to authorize the user to select several regions of interest and to apply, on each of them, different pre-processings and different adjustments of parameters for the PIV-processing. This software limited the amount of user manipulations and so, saved time.

3.1. PRE-PROCESSING

The main issue was that vibrations induced displacements between pairs of images. That prevented from launching automatic processings over a large range of images. Indeed, because of this displacement, region of interest the user selected was not at the same spatial localization on each image. For that reason, we developed pre-processing operation to shift all the images so that they all had the same spatial origin.

During a same experiment, displacements larger than 20 pixels were observed between different pairs of images. Nevertheless, it was not the case between 2 images belonging to the same pair. Indeed, the delay time between 2 images of a single pair was short enough so that translation due to vibrations was not visible. Thus, the shifting operation involved determining relative displacement between an image from a pair of reference, and another one from a pair to process. The displacement calculation was done performing a classical PIV correlation process [9]. More precisely, an interrogation area (Zref) with a fixed pattern was selected on the image of reference. Zref had coordinates (x, y) and size (dx, dy). Then the same interrogation area Zi was selected on images to process. On each of them, Zi had the same coordinates (x, y) and size (dx, dy) than Zref. Correlation between Zref and each Zi gave the relative displacement between each pair of images and the reference one. After this calculation, all images were shifted to match the same origin than the reference.

Even if this shifting operation was automatic for a range of images, it was necessary to perform this twice for each experiment since there were 2 cameras so 2 distinct ranges of images. Once all images were shifted so that they all had the same spatial origin, it was possible to select regions of interest and to apply some pre-processing and PIV-processing operations.

The use of optical reflectors to obtain images of 4 runners on each camera induced orientations modifications. Distinct flips and rotations operations could be applied to each selected regions (corresponding to each runner) in order to correct orientations of the runners' images.

To limit influence of remaining reflections, it was possible to calculate an average image from non-seeded acquisitions to obtain a background image that was subtracted to images.

3.2. PIV-PROCESSING

Two kinds of processings were available, both based on cross-correlation. The first one was the classical PIV-processing based on cross-correlation and a 3-points Gaussian fitting of the maximum correlation peak. The second one is based on cross-correlation and window offset as proposed by [10] with 3-points Gaussian fitting. This algorithm took advantage of results from a first correlation between interrogation areas that gave displacements in integer pixels. Then, interrogation areas from the second image were shifted according to these displacements. Then, a second correlation processing was applied and coupled with 3-points Gaussian fitting to obtain more accurate displacements.

For each method, the user chose several parameters. He defined size (Dx, Dy) as well as overlap (dx, dy) of interrogation areas that meshed regions of interest. Overlap was a tuple of integer greater or equal to 1 that can be greater than interrogation areas size. Spatial calibrations parameters for 2 components x and y as well as the delay time were filled in to convert particles displacements into velocities. Considering window offset algorithm, the user had to input size (D'x, D'y) of interrogation areas for the second correlation processing, so that they could have been smaller or larger than size (Dx, Dy) of the first processing.

There were two ways of saving results. Results from every regions of interest were saved independently, or they were saved in the same file. This last type of saving was useful when wanted to apply different kind of processings inside different regions of the flow (for instance, a processing for the region of a flow in the middle of a working section, and a different one for the boundary layer).

4. CODE VALIDATION

To evaluate the accuracy of the PYV software process, we chose to numerically generate images [11]. Parameters of these images, and particles displacements were perfectly known. Thus, a direct comparison between imposed displacement fields and those obtained by the PIV processing were made. From this comparison, mean bias error and standard deviation can be determined. For each run, 1000 images (32x32 pix^2 and 8 bits coded) were generated taking into account several criterions. Concerning the image quality on the CCD, no noise was added, the percentage of active surface was set at 100%, and its black level set at 0%.

The first criterion was the characteristics of particles. Their 3D positions in the image A were randomly determined, following a continuous uniform distribution. Particles positions in image B were imposed by applying a uniform displacement field to particles in image A (neither displacement gradient, nor displacement in the laser sheet width direction). Various displacements values were tested: from 0 to 2 pix by steps of 0.05 pix.

The variation of the luminous intensity of a particle I_p as a function of the distance from the center of the particle r was defined following a Gaussian function:

$$I_p(r) = I_{max}.e^{-\frac{r^2}{\frac{1}{8}d_p^2}}$$

The particle diameter, d_p, corresponded to two times the distance from the center of the particle for which the Gaussian is equal to "$e^{-2}.I_{max}$", with I_{max} the maximum of the Gaussian.

Particle diameters were randomly obtained, following a normal distribution with a mean diameter of 2 pix at e^{-2}, and an associated standard deviation equal to $\frac{\overline{d_p}}{4}$.

Last important parameters were luminous intensities of each particles on image A and B (which depends on laser sheet intensity profile) and particle seeding density, which was set at 0.039 pix^{-2}. We used a Gaussian laser sheet intensity profile for the sheet's width. This last one was equal to 5 pix at e^{-2}. An example of generated images is given on the Figure 4.

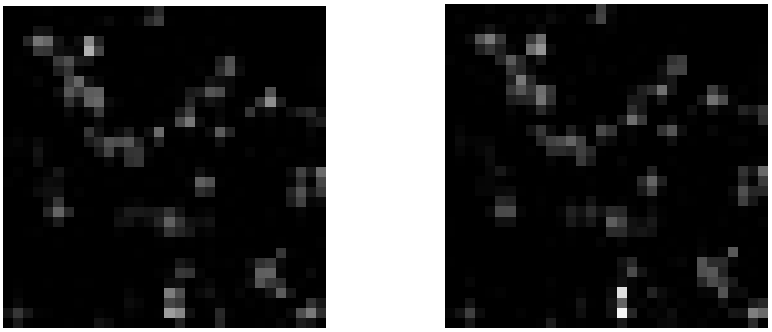

Figure 4 Example of a pair of images generated (Size: 32x32pix^2, displacement of each particle: 0.5 pix in the horizontal direction).

Then, the generated images were tested using the PYV software, for a FFT-based cross-correlation algorithm with a 3 points interpolation of the Gaussian peak. For each test, we represented both bias error B and standard deviation σ.

$$B = \frac{1}{N}\sum_{i=1}^{N}(D_{ci} - D_r) = \overline{D_c} - D_r \qquad \sigma = \sqrt{\frac{1}{N}\sum_{i=1}^{N}(D_{ci} - \overline{D_c})^2}$$

With D_r the real displacement, N the number of calculated displacement (D_{ci}), and $\overline{D_c}$ the average of the calculated displacements.

The Figure 5 gives bias error and standard deviation for a classic correlation process (a), and for an iterative process with window offset (b).

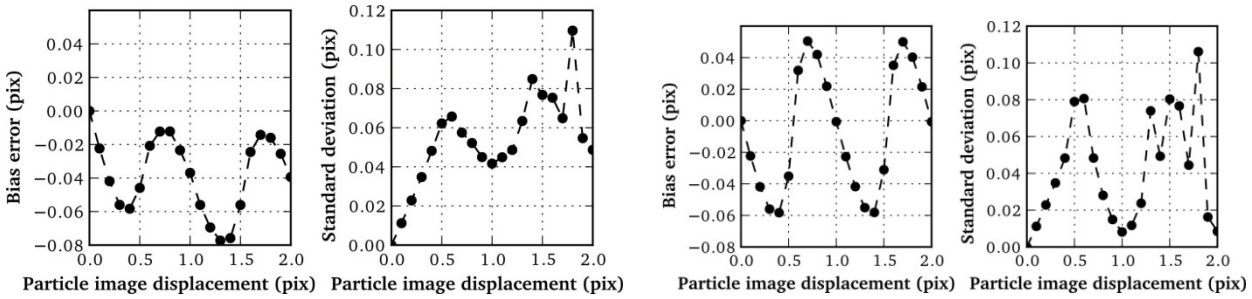

(a) Classic correlation process (b) Iterative process with sliding windows

Figure 5 Bias error and standard deviation.

For all our tests, we found that the bias error was below 0.08 pix. For typical adjustment of PIV parameters (i.e. particles displacements between 1/4 or 1/3 of the interrogation area) on interrogation windows of 16x16 pix^2, the maximum error on the velocity would be equal to 1.5%. This error would decrease when increasing size of the interrogation area. All these results enabled us to conclude that the process of PYV software delivered good results, and thus to validate our code.

5. RESULTS

Experimental setup enabled to acquire images from 4 runners on each camera, and thus images from 8 runners were recorded simultaneously. An example of an image obtained on one camera is presented on Figure 6. Identical laser sheets in the four runners are visible. As previously mentioned, the engine vibrations had an impact on recorded images which had to be corrected. On the Figure 7, an example of the selection of the same region on two different images is given. The images (a) corresponded to results without preprocessing. On the right of this figure, the displacement of the bright edge is obvious. Images (b) corresponds to the same region selected, but after the pre-processing shifting operation described earlier (cf. § 3.1). In this last case, the luminous right edge is located at the same position, showing that the shifting operation was successful. Before image shifting, one can observe bright borders on the right are not at the same position. This is due to vibrations that induced a displacement between acquisitions. After the shifting operation, images have the same spatial origin and position.

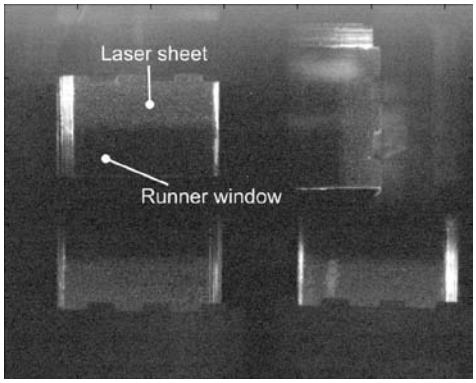

Figure 6 Example of acquired image on 1 camera. 4 laser sheets into runners are visible.

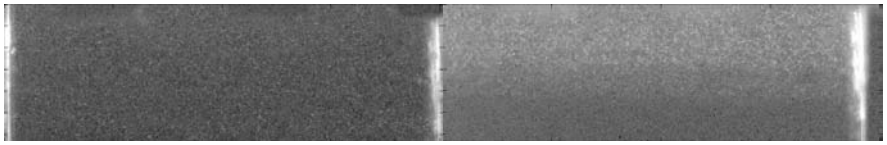

(a) Before image shifting.

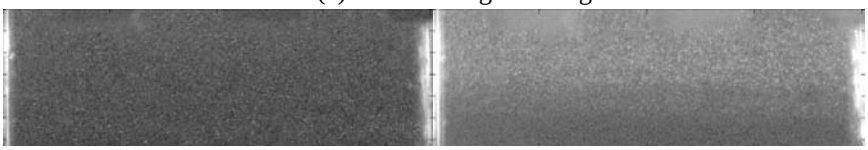

(b))After shifting operation

Figure 7 Example showing to selections of the same region for different acquisitions.

Once all the images shifted and their orientation corrected (flips and/or rotation), four regions of interest (corresponding to the laser sheet in the four runners) were defined on the images. The PIV process was applied and, for each crank angle, instantaneous velocity vector fields were obtained. The figure 8 represents the height instantaneous velocity vector fields obtained simultaneously in the eight runners for a crank angle of 90°. In that case, the engine was running at 2000 rpm with a load of 70 N.m. We selected this crank angle since it corresponded to the one for which the velocity was maximal in two runners, and almost null in the six other runners.

Mean discharge velocities were then calculated for every of the 720 crank angle degrees. These results are presented on Figure 9, where velocity curves are drawn versus crank angle for every runner. On these curves, negative velocities corresponded to the flow entering into cylinder. One can observe a main velocity peak for each runner curve, which is relative to corresponding intake valve opening.

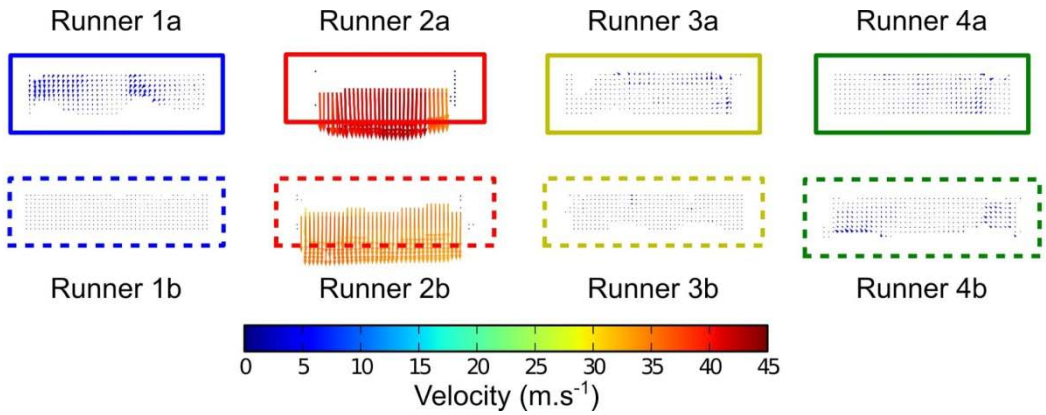

Figure 8 Instantaneous velocity vectors fields in the 8 runners, for a crank angle of 90°. Speed and load of the running engine: 2000 rpm - 70 N.m.

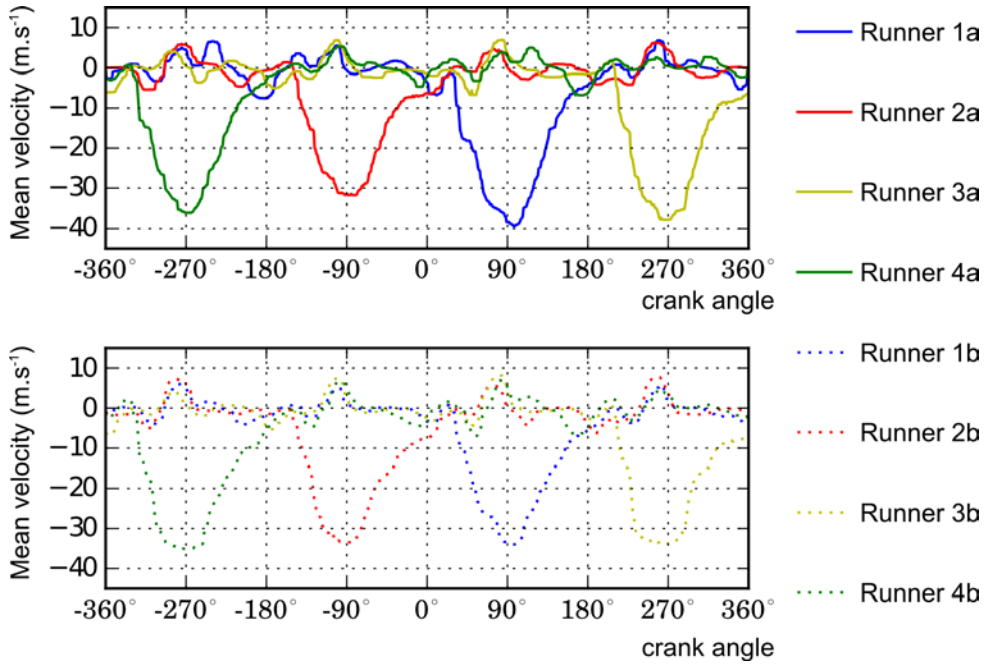

Figure 9 Mean velocity versus crank angle in the 8 runners of the intake manifold (2000 rpm 70 N.m)

6. CONCLUSION

A PIV experimental setup, as well as its associated "PYV" software which allowed to determine the velocity inside intake manifold runners, were presented. Simultaneous measurements inside 8 runners were performed on a real running engine at a representative engine speed of 2000 rpm and a load of 70 N.m. Thus, velocities were obtained for each single degree of the 720 crank angle ones. This was made possible first thanks to the experimental setup that dealt with most of the constraints of such a severe environment. Second, a processing tool was developed, among other reasons, to deal with remaining issues. It allowed to measure global image displacements due to vibrations in order to shift all the images at the same spatial origin. Thus, it was possible to automatically apply pre-processings and PIV-processings over different regions of interest. Thanks to these tools, it was possible to realize optical PIV measurements and obtain instantaneous velocity vector fields in the eight runners of the intake manifold of a real a running engine.

ACKNOLEDGEMENTS

This work is supported by the research project SIMBA funded by "l'Etat Français" (Contract No.072906524) and by the "Communauté d'agglomération du Pays de Montbéliard". Experiments were achieved in the R&D Moteur's test facility CEMBA.

REFERENCES

[1] Weclas M, Melling A and Durst F "Flow separation in the inlet valve gap of piston engines" Progress in Energy and Combustion Science 24.3 (1998) pp 165 –195

[2] Guibert P and Le Moyne L "Dual particle image velocimetry for transient flow field measurements" Experiments in Fluids 33 (2002) pp 355–367

[3] Voisine M, Thomas L, Borée J and Rey P "Etude par PIV de la structuration tridimensionnelle moyenne et des fluctuations cycle à cycle d'une aérodynamique interne moteur de type rouleau" Proceedings of Congrès Francophone de Techniques Laser (2008) pp 16–19

[4] Borée J "Analyse statistique des cohérences spatiales et spatio-temporelles en moteur à piston. Outils et applications." Proceedings of Congrès Francophone de Techniques Laser (2012) pp 25–28

[5] Towers DP and Towers CE "Cyclic variability measurements of in-cylinder engine flows using high-speed particle image velocimetry". Measurement Science and Technology 15.9 (2004) pp 1917

[6] Bonnet D, Barthès M, Ramel D, Girardot L, Bailly Y, Guermeur F, Guyon D, Grenier A, Perrot Y and Ragot D “Vélocimétrie par PIV d'écoulements pulsés instationnaires sur banc moteur industriel” Proceedings of Congrès de Mesures et Techniques Optiques pour l’Industrie (2010)

[7] Le Moyne L, Maroteaux F, Guibert P and Murat M “Model and Measure of Flows at the Intake of Engines” Journal de Physique III 7.10, (1997). pp 1927–1940

[8] Justham T, Jarvis S, Clarke A, Garner CP, Hargrave GK and Halliwell NA “Simultaneous study of intake and in-cylinder IC engine flow fields to provide an insight into intake induced cyclic variations” Journal of Physics : Conference Series. T. 45. IOP Publishing, (2006) pp 146.

[9] Raffel M, Willert CE and Kompenhans J “Particle image velocimetry, a practical guide” Springer, Berlin (1998)

[10] Westerweel J, Dabiri D and Gharib M “The effect of a discrete window offset on the accuracy of cross-correlation analysis of digital PIV recordings” Experiments in Fluids 23 (1997) pp. 20-28

[11] Foucault JM, Miliat B, Perenne N and Stanislas M. “Characterization of different PIV algorithms using the EUROPIV synthetic image generator and real images from a turbulent boundary layer” Proceedings of the EUROPIV 2 (2004) pp. 163-185